Transition Met Chem
DOI 10.1007/s11243-014-9810-4

# Synthesis and electrochemistry of phenyl-functionalized diiron propanedithiolate complexes with bidentate phosphine ligands

**Chang-Gong Li · Yong-Fang Li · Jing-Yan Shang · Tian-Jun Lou**

Received: 9 December 2013 / Accepted: 18 February 2014


**Abstract** Carbonyl substitution reactions of $[\mu\text{-}(SCH_2)_2\text{-}CHC_6H_5]Fe_2(CO)_6$ with bidentate phosphine ligands, *cis*-1,2-bis(diphenylphosphine)ethylene (*cis*-dppv) and *N*,*N*-bis(diphenylphosphine)propylamine $[(Ph_2P)_2N\text{-}Pr\text{-}n]$, yielded an asymmetrically substituted chelated complex $[(\mu\text{-}SCH_2)_2\text{-}CHC_6H_5]Fe_2(CO)_4(k^2\text{-dppv})$ and a symmetrically substituted bridging complex $[(\mu\text{-}SCH_2)_2CHC_6H_5]Fe_2(CO)_4[\mu\text{-}(PPh_2)_2\text{-}N\text{-}Pr\text{-}n]$ under different reaction conditions. Both complexes were fully characterized by spectroscopic methods and by X-ray crystallography. Their electrochemical behaviors were observed by cyclic voltammetry, and the catalytic electrochemical reduction of protons from acetic or trifluoroacetic acid to give dihydrogen mediated by complex $[(\mu\text{-}SCH_2)_2\text{-}CHC_6H_5]Fe_2(CO)_4(k^2\text{-dppv})$ was investigated.

## Introduction

FeFe-hydrogenases can efficiently catalyze the reduction of protons to dihydrogen or vice versa in a variety of microorganisms [1–3]. The active site structures of FeFe-hydrogenases (H-cluster) have been revealed by X-ray crystallographic [4–6] and FTIR spectroscopic [7–9] studies, in which one of the two iron atoms of the [2Fe2S] butterfly cluster is linked to a cubic [4Fe4S] cluster by the sulfur atom of a cysteine ligand, while a dithiolate cofactor ($SCH_2XCH_2S$; X = N, C or O) bridges the two iron atoms, which are also coordinated by CO and $CN^-$ ligands. Therefore, much attention has been directed to butterfly- and cubane-like Fe/S cluster complexes in view of their structural and functional similarity with the active sites of FeFe-hydrogenases [10, 11]. Since both iron and sulfur are widely available and relatively abundant elements in the crust of our planet, it is hoped that an exploration of the biomimetic chemistry of FeFe-hydrogenases may lead to cheap and efficient iron-based hydrogen production catalysts, instead of precious metal platinum or palladium catalysts [12–14]. During the investigation of the bioinspired chemistry of FeFe-hydrogenases, the classical diiron dithiolate complexes, $[(\mu\text{-pdt})Fe_2(CO)_6]$ (pdt = $SCH_2CH_2CH_2S$) [15] and $[(\mu\text{-adt})Fe_2(CO)_6]$ (adt = $SCH_2NHCH_2S$) [16], became the focus of much research [17–20]. A theoretical study by Tye, Darensbourg and Hall concluded that "asymmetric substitution of strong donor ligands is the most viable method of making better synthetic diiron complexes that will serve as both structural and functional models" of the active site of iron-only hydrogenase [21]. As part of our ongoing research centered on phenyl-functionalized diiron propanedithiolate complexes [22], in this paper we describe asymmetrical and symmetrical model complexes corresponding to replacement of carbonyls by bidentate phosphine ligands, namely *cis*-1,2-bis(diphenylphosphine)ethylene (*cis*-dppv) and *N*,*N*-bis(diphenylphosphine)propylamine $[(Ph_2P)_2N\text{-}Pr\text{-}n]$. The two complexes were formulated as $[(\mu\text{-}SCH_2)_2CHC_6H_5]Fe_2(CO)_4(k^2\text{-dppv})$ (**1**) and $[(\mu\text{-}SCH_2)_2CHC_6H_5]Fe_2(CO)_4[\mu\text{-}(PPh_2)_2N\text{-}Pr\text{-}n]$ (**2**). The electrochemical behaviors of both complexes and the electrochemical reduction of protons catalyzed by complex **1** were investigated.

C.-G. Li (✉) · Y.-F. Li · J.-Y. Shang
College of Chemistry and Chemical Engineering, Henan Institute of Science and Technology, Xinxiang 453003, People's Republic of China
e-mail: lichanggong@sohu.com

T.-J. Lou
Xinxiang Municipal Key Laboratory of Functional Organic Molecular, Xinxiang 453003, People's Republic of China

Published online: 01 March 2014

## Experimental

### Materials and methods

All reactions and operations were carried out under a dry, oxygen-free argon atmosphere using standard Schlenk and vacuum line techniques. $CH_2Cl_2$ and MeCN were distilled from $CaH_2$, while *n*-hexane, xylene and toluene were purified by distillation from sodium/diphenylmethanone under argon. $Me_3NO{\cdot}2H_2O$ and *cis*-dppv were commercially available and used as received. $(Ph_2P)_2N$-Pr-*n* [23] and $[\mu\text{-}(SCH_2)_2CHC_6H_5]Fe_2(CO)_6$ [22] were prepared according to literature methods. Preparative TLC was carried out on glass plates (25 cm × 20 cm × 0.25 cm) coated with silica gel G (10–40 μm). IR spectra were recorded on a Bruker TENSOR 27 FTIR spectrometer. $^1H$, $^{13}C$ and $^{31}P$ NMR spectra were obtained on a Bruker Avance 400 MHz spectrometer. Elemental analyses were performed on an Elementar Vario EL III analyzer.

### Electrochemistry

Electrochemical measurements were carried out using a CHI 620 Electrochemical Workstation (CH Instruments, Chenhua, Shanghai, China). A solution of 0.1 M $n\text{-}Bu_4NPF_6$ in $CH_3CN$ was used as the electrolyte, degassed by bubbling with dry nitrogen for 10 min before measurement. CV scans were obtained in a three-electrode cell with a glassy carbon electrode (3 mm diameter) as the working electrode, successively polished with 3 and 1 μm diamond pastes and sonicated in ion-free water for 1 min, a platinum wire as counter electrode, and a nonaqueous $Ag/Ag^+$ electrode (1.0 mM $AgNO_3$ and 0.1 M $n\text{-}Bu_4NPF_6$ in $CH_3CN$) as reference. The potential scale was calibrated against the $Fc/Fc^+$ couple and reported versus this reference system.

### X-ray structure determination

Single crystals of both complexes suitable for X-ray diffraction analysis were grown by slow evaporation of the $CH_2Cl_2$/hexane solutions at 5 °C. For each complex, a suitable crystal was selected and analyzed on an Xcalibur, Eos, Gemini diffractometer. The crystal was kept at 291.15 K during data collection. Using Olex2 [24], the structure was solved with the ShelXS structure solution program using direct Methods and refined with the ShelXL refinement package using least-squares minimization [25]. The program SQUEEZE was employed to squeeze out hexane, which was disordered beyond recognition. Details of crystal data, data collections and structure refinement are summarized in Table 1.

**Table 1** Crystal data and structural refinements for complexes **1** and **2**

| | **1** | **2** |
|---|---|---|
| Empirical formula | $C_{39}H_{32}Fe_2O_4P_2S_2$ | $C_{40}H_{37}Fe_2NO_4P_2S_2$ |
| Formula weight | 802.41 | 833.47 |
| Temperature/K | 291.15 | 291.15 |
| Crystal system | Monoclinic | Monoclinic |
| Space group | $P2_1/n$ | $P2_1/n$ |
| $a$/Å | 10.98620(11) | 15.2539(3) |
| $b$/Å | 10.90100(9) | 17.5816(4) |
| $c$/Å | 30.9101(3) | 16.7714(3) |
| $\alpha$/° | 90.00 | 90.00 |
| $\beta$/° | 90.5358(8) | 99.3578(19) |
| $\gamma$/° | 90.00 | 90.00 |
| $V$/Å$^3$ | 3701.65(6) | 4438.02(17) |
| $Z$ | 4 | 4 |
| $D$/g mm$^{-3}$ | 1.440 | 1.247 |
| $\mu$/mm$^{-1}$ | 8.477 | 7.094 |
| $F$(000) | 1,648.0 | 1,720.0 |
| Crystal size/mm$^3$ | 0.25 × 0.2 × 0.17 | 0.22 × 0.2 × 0.2 |
| $2\theta$ Range for data collection/° | 5.72–134.16 | 7.26–134.12 |
| Index ranges | $-12 \le h \le 13$<br>$-13 \le k \le 8$<br>$-36 \le l \le 34$ | $-12 \le h \le 18$<br>$-18 \le k \le 20$<br>$-20 \le l \le 19$ |
| Reflections collected | 13,886 | 15,966 |
| Independent reflections ($R_{int}$) | 6,604 (0.0225) | 7,904 (0.0496) |
| Data/restraints/parameters | 6,604/0/442 | 7,904/0/461 |
| Goodness-of-fit on $F^2$ | 1.031 | 1.029 |
| Final R indexes [$I > 2\sigma$ ($I$)] | $R_1 = 0.0352$; $wR_2 = 0.0883$ | $R_1 = 0.0495$; $wR_2 = 0.1210$ |
| Final R indexes [all data] | $R_1 = 0.0410$; $wR_2 = 0.0919$ | $R_1 = 0.0728$; $wR_2 = 0.1296$ |
| Largest diff. peak/hole/e Å$^{-3}$ | 0.32/−0.43 | 0.64/−0.34 |

### Synthesis of complex 1

$[\mu\text{-}(SCH_2)_2CHC_6H_5]Fe_2(CO)_6$ (0.08 g, 0.17 mmol) was dissolved in toluene (10 mL) under argon, and $Me_3NO{\cdot}2H_2O$ (0.02 g, 0.18 mmol) in MeCN (5 mL) was added. The red solution became brown immediately. After stirring at room temperature for ca. 10 min, a solution of *cis*-dppv (0.075 g, 0.19 mmol) in toluene (10 mL) was added and the mixture was stirred at room temperature for 3 h. The solvent was removed on a rotary evaporator, and the residue was subjected to preparative TLC separation using $CH_2Cl_2$/petroleum ether (v/v = 1:2) as eluent. From the brown band, complex **1** was obtained as a brown-black solid (0.122 g, 90 %). IR (KBr disk, cm$^{-1}$): $\nu_{C\equiv O}$ 2,014

(vs), 1,941 (vs), 1,930 (vs), 1,905 (vs). $^{1}$H NMR (400 MHz, $CDCl_3$, ppm): 1.777–1.927 (m, 3H, 2 SC*Ha*He, PhC*H*), 2.414 (m, 2H, 2 SCHa*He*), 6.152 (d, 2H, 2 = C*H*, $^{3}J = 2.8$ Hz), 7.033–7.867 (m, 25H, Ph*H*). $^{13}$C NMR (400 MHz, $CDCl_3$, ppm): 207.8 (s, FeCO), 132.8, 132.7, 130.4, 130.0, 128.7, 128.5, 128.3, 126.4 (s, PhC), 48.7 (s, CH), 31.1 (s, $SCH_2$). $^{31}$P NMR (161.9 MHz, $CDCl_3$, 85 % $H_3PO_4$, ppm): 90 (s, 92 %, basal–apical), 78 (s, 8 %, basal–basal). Anal. Calc. for $C_{39}H_{32}Fe_2O_4P_2S_2$: C, 58.4; H, 4.0. Found: C, 58.6; H, 3.8 %.

### Synthesis of complex 2

A xylene (15 mL) solution of [$\mu$-$(SCH_2)_2CHC_6H_5$]$Fe_2(CO)_6$ (0.143 g, 0.31 mmol) and $(PPh_2)_2$N-Pr-*n* (0.133 g, 0.31 mmol) was refluxed for 3 h. After removing the solvent under reduced pressure, the crude product was purified by chromatography on silica gel using $CH_2Cl_2$/petroleum ether (v/v = 1:1) as eluent. Complex **2** was obtained as a red solid (0.077 g, 30 %). IR (KBr disk, $cm^{-1}$): $\nu_{C\equiv O}$ 1,994 (vs), 1,961 (vs), 1,924 (vs). $^{1}$H NMR (400 MHz, $CDCl_3$, ppm): 0.053 (s, 3H, $NCH_2CH_2CH_3$), 0.292 (m, 2H, $NCH_2CH_2CH_3$), 1.803 (s, 2H, $NCH_2CH_2CH_3$), 2.529–2.677 (m, 5H, $SCH_2CHCH_2S$), 7.079–7.718 (m, 25H, Ph*H*). $^{13}$C NMR (400 MHz, $CDCl_3$, ppm): 216.1 (s, FeCO), 148.0, 133.2, 132.3, 132.0, 130.4, 128.6, 128.0, 127.7, 127.0 (s, PhC), 54.4, 53.5, 50.1, 31.6, 22.9, 11.0 (s, CH, $CH_2$, $CH_3$). $^{31}$P NMR (161.9 MHz, $CDCl_3$, 85 % $H_3PO_4$, ppm): 119 (s). Anal. Calc. for $C_{40}H_{37}Fe_2NO_4P_2S_2$: C, 57.6; H, 4.5, N, 1.7. Found: C, 57.5; H, 4.2, N, 1.9 %.

## Results and discussion

### Synthesis and spectroscopic characterization

As shown in Scheme 1, the reaction of the precursor complex [$\mu$-$(SCH_2)_2CHC_6H_5$]$Fe_2(CO)_6$ with ca. 1 equivalent of the decarbonylating agent $Me_3NO{\cdot}2H_2O$ followed by addition of 1.1 equivalent of *cis*-dppv at room temperature gave the chelated complex **1**, while refluxing a xylene solution of the precursor complex [$\mu$-$(SCH_2)_2CHC_6H_5$]$Fe_2(CO)_6$ with 1 equiv of $(Ph_2P)_2$N-Pr-*n* yielded the bridged complex **2**. Compared with the IR absorption bands of the terminal carbonyls of the precursor complex (2,071, 2,022, 2,008, 1,970 $cm^{-1}$), those of complexes **1** and **2** were considerably shifted by about 60–80 $cm^{-1}$ toward lower energy. This is apparently due to two CO ligands being replaced by stronger electron-donating diphosphine ligands [26]. The biggest absorption band of the terminal carbonyls at 2,014 $cm^{-1}$ for complex **1** corresponds to substitution of the two carbonyls by the chelating diphosphine, while the band observed at 1,994 $cm^{-1}$ for complex **2** is consistent with substitution of the two carbonyls with diphosphine in a bridging coordination geometry [27]. In the $^{1}$H NMR spectra, compared with the chemical shifts of the propanedithiolate bridge protons of the precursor complex [$\mu$-$(SCH_2)_2CHC_6H_5$]$Fe_2(CO)_6$, those of complex **1** showed upfield shifts, whereas those of complex **2** were little changed. These observations imply that coordination of phosphine ligands not only increases the electron density of the diiron centers, but also indirectly affects other ligands depending on the nature of the coordination sphere. The upfield shift signals of the *n*-Pr protons in complex **2** are due to the shielding effect of the benzene rings [28]. The $^{13}$C NMR spectra showed weak resonances from the carbonyl carbon atoms at ca. 210 ppm, strong olefin carbon signals in the range of 126–148 ppm and alkane carbon signals in the range of 11–54 ppm. The $^{31}$P NMR spectra showed two singlets at 90 and 78 ppm for the phosphorus atoms of the *cis*-dppv ligand in complex **1** with a ratio of ca. 92:8, corresponding to apical–basal and basal–basal chelating coordination patterns, whereas that of complex **2** displayed one singlet at 119 ppm, consistent with symmetrical coordination of the two nitrogen-binding phosphine atoms to two iron atoms in a basal–basal coordination manner.

### X-ray crystal structures

The molecular structures of both complexes were unambiguously confirmed by X-ray crystallography (Figs. 1, 2), and crystal data, selected bond lengths and angles are listed in Tables 1 and 2. Both complexes each have a butterfly [2Fe2S] core in which their two iron atoms are bridged by a 2-phenyl-1, 3-propanedithiolate ligand. One of the two Fe atoms and the propanedithiolate bridge form a six-membered ring in chair conformation, with the phenyl group in an equatorial position. The Fe–Fe bond length of complex **1** (2.5517(5) Å) is much longer than that of complex **2** (2.4851(9) Å) and close to those found in the reduced active site of FeFe-hydrogenases [6]. The two phosphine atoms of *cis*-dppv chelate one of the two iron atoms with an apical–basal coordination geometry, whereas the two phosphine atoms of $(Ph_2P)_2$N-Pr-*n* coordinate two iron atoms with a bridging basal–basal manner. The bite angle P2–Fe2–P1 is 87.83(5)° for complex **1**, close to those of [($\mu$-$SCH_2)_2$]$Fe_2(CO)_4$($\kappa^2$-dppv) [29, 30]. Two phosphine atoms and two carbon atoms of *cis*-dppv ligand, and the Fe2 atom in complex **1** constitute a five-membered ring with dihedral angle of 15.2 (1)° between the plane (P2, Fe2, P1) and the plane (P1, C26, C27), and a torsion angle of 3.6 (8)° between P2 and P1. In the five-membered ring of complex **2**, the dihedral angle between planes (P1, N1, P2) and (N1, P1, Fe1) is 10.8 (7)°, and four atoms, P2, P1, Fe1 and Fe2, are almost co-planar.

**Scheme 1** Preparation of complexes **1** and **2**

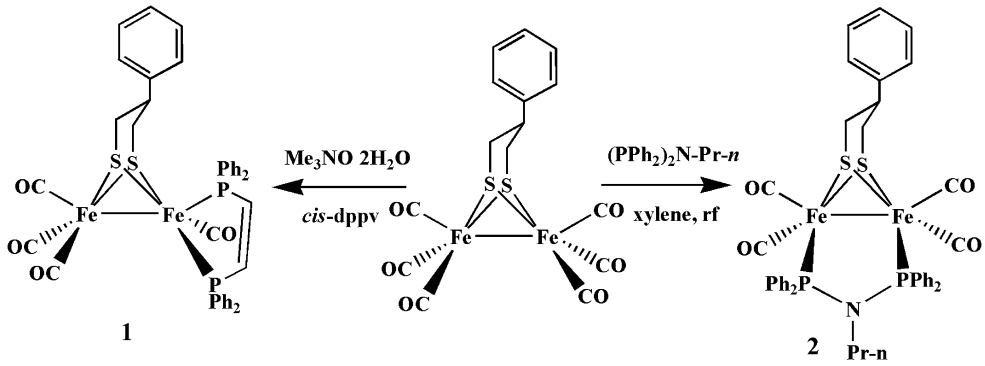


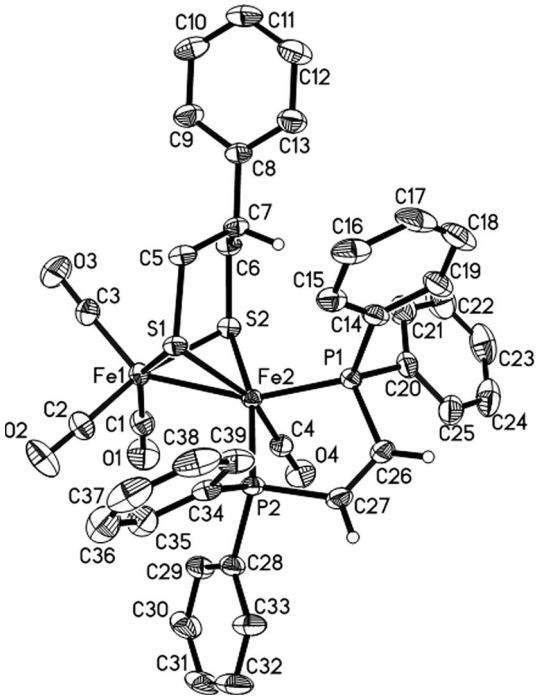

**Fig. 1** Molecular structure of complex **1** with thermal ellipsoids at 30 % probability

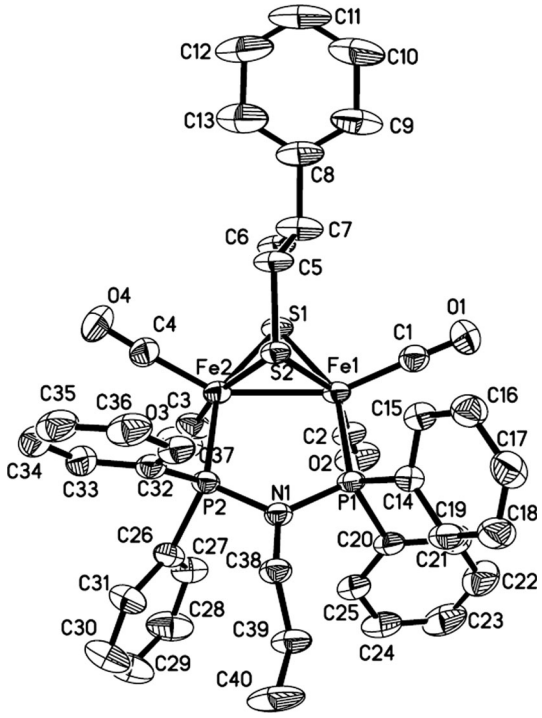

**Fig. 2** Molecular structure of complex **2** with thermal ellipsoids at 30 % probability

## Electrochemistry

The cyclic voltammograms of both complexes were recorded and are shown in Figs. 3, 4 and 5. Complex **1** displays two irreversible reduction processes at −2.106 and −2.542 V, and one quasi-reversible oxidation process at +0.014 V, which are assigned to the reductions of $Fe^{I}Fe^{I}$ to $Fe^{I}Fe^{0}$ and $Fe^{I}Fe^{0}$ to $Fe^{0}Fe^{0}$, and the oxidation of $Fe^{I}Fe^{I}$ to $Fe^{I}Fe^{II}$, respectively. The reduction potentials of complex **1** are negatively shifted by 0.46 V compared to the corresponding reduction potentials of the precursor complex [$\mu$-$(SCH_2)_2CHC_6H_5]Fe_2(CO)_6$ [22], due to its two CO ligands being replaced by the stronger electron-donating ligand. For complex **1**, after addition of trifluoroacetic acid (1 equiv.), a new reduction process was observed at −1.875 V, positively shifted by about 0.2 V compared with the reduction potential at −2.106 V in the absence of trifluoroacetic acid. With increasing concentration of trifluoroacetic acid, the current intensity of the new reduction potential at −1.875 V grew dramatically and the reduction potential moved from −1.875 V to more negative reduction potential at −2.413 V. The current intensity of the reduction potential at −2.106 V showed little change and was obscured with increasing concentration of trifluoroacetic acid (Fig. 3). In the presence of acetic acid, the current intensities of the two reduction potentials at −2.106 and −2.542 V increased slightly (Fig. 4, 1 and 2 mM acetic acid), while a new reduction process at −2.355 V was observed for 4 mM acetic acid, and its current intensity grew markedly with the further increment of acetic

**Table 2** Selected bond lengths (Å) and angles (deg) for complexes **1** and **2**

| | | | | | | | |
|---|---|---|---|---|---|---|---|
| ***1*** | | | | | | | |
| Fe(1)–Fe(2) | 2.5517(5) | Fe(2)–P(1) | 2.1797(7) | Fe(2)–S(2) | 2.2459(6) | C(26)–C(27) | 1.316(4) |
| Fe(1)–S(1) | 2.2632(7) | Fe(2)–P(2) | 2.2123(6) | S(1)–C(5) | 1.839(2) | O(4)–C(4) | 1.149(3) |
| Fe(1)–S(2) | 2.2712(7) | Fe(2)–S(1) | 2.2566(6) | S(2)–C(6) | 1.825(2) | Fe(1)–C(1) | 1.796(3) |
| O(1)–C(1) | 1.137(4) | O(2)–C(2) | 1.132(4) | O(3)–C(3) | 1.141(4) | Fe(2)–C4 | 1.756(3) |
| S(1)–Fe(1)–S(2) | 84.29(2) | S(2)–Fe(2)–S(1) | 85.02(2) | Fe(2)–S(1)–Fe(1) | 68.743(19) | S(2)–Fe(1)–Fe(2) | 55.137(17) |
| S(1)–Fe(1)–Fe(2) | 55.506(17) | S(1)–Fe(2)–Fe(1) | 55.750(18) | Fe(2)–S(2)–Fe(1) | 68.79(2) | S(2)–Fe(2)–Fe(1) | 56.075(18) |
| P(1)–Fe(2)–P(2) | 87.31(2) | P(1)–Fe(2)–Fe(1) | 157.35(2) | P(1)–Fe(2)–S(1) | 111.99(3) | P(1)–Fe(2)–S(2) | 107.15(3) |
| P(2)–Fe(2)–Fe(1) | 110.86(2) | P(2)–Fe(2)–S(1) | 92.75(2) | P(2)–Fe(2)–S(2) | 165.16(3) | C(4)–Fe(2)–P(2) | 89.22(9) |
| C(4)–Fe(2)–P(1) | 90.31(8) | C(3)–Fe(1)–Fe(2) | 143.63(10) | C(1)–Fe(1)–Fe(2) | 97.94(9) | C(3)–Fe(1)–C(1) | 104.75(14) |
| ***2*** | | | | | | | |
| Fe(1)–Fe(2) | 2.4851(9) | Fe(1)–S(1) | 2.2580(12) | Fe(1)–S(2) | 2.2564(10) | Fe(1)–C(1) | 1.764(5) |
| Fe(1)–P(1) | 2.2097(11) | P(1)–N(1) | 1.713(3) | Fe(2)–S(2) | 2.2574(12) | O(1)–C(1) | 1.148(5) |
| Fe(2)–P(2) | 2.2180(11) | P(2)–N(1) | 1.719(3) | Fe(2)–S(1) | 2.2505(11) | Fe(2)–C(4) | 1.764(4) |
| S(1)–Fe(1)–Fe(2) | 56.41(3) | S(1)–Fe(2)–Fe(1) | 56.70(3) | S(2)–Fe(1)–S(1) | 84.61(4) | Fe(2)–S(1)–Fe(1) | 66.90(3) |
| S(2)–Fe(1)–Fe(2) | 56.61(3) | S(1)–Fe(2)–S(2) | 84.76(4) | S(2)–Fe(2)–Fe(1) | 56.58(3) | Fe(1)–S(2)–Fe(2) | 66.81(3) |
| P(1)–Fe(1)–Fe(2) | 97.25(3) | P(1)–N(1)–P(2) | 118.48(18) | C(1)–Fe(1)–P(1) | 98.86(15) | C(2)–Fe(1)–P(1) | 92.37(14) |
| P(2)–Fe(2)–Fe(1) | 94.79(4) | C(4)–Fe(2)–P(2) | 100.82(15) | C(3)–Fe(2)–P(2) | 96.85(14) | C(4)–Fe(2)–Fe(1) | 147.93(17) |

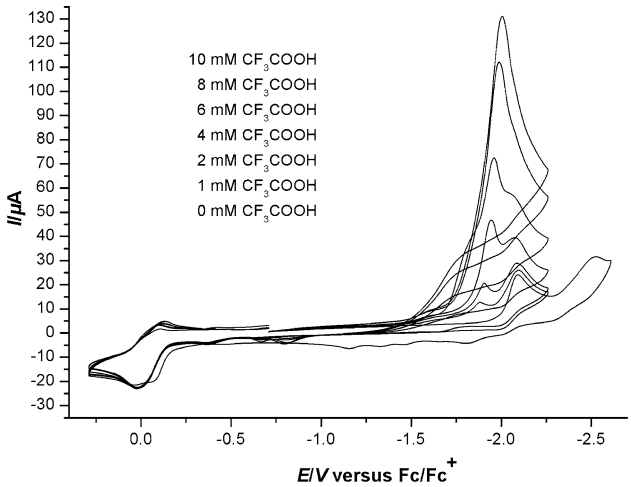


**Fig. 3** Cyclic voltammetry of complex **1** (1 mM) in 0.1 M *n*-$Bu_4NPF_6$/MeCN with and without $CF_3COOH$ (0–10 mM) at a scan rate of 0.1 V $s^{-1}$

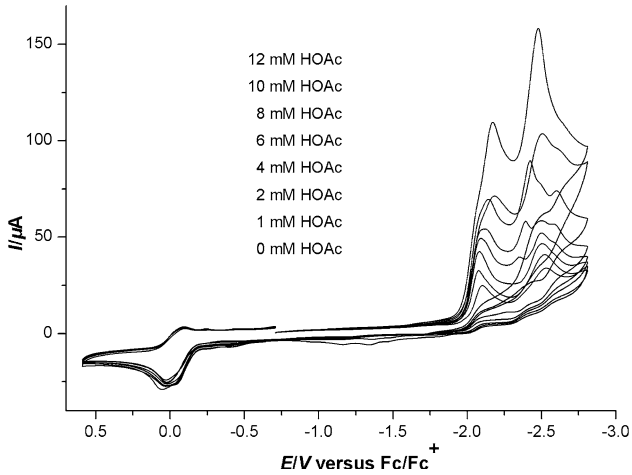


**Fig. 4** Cyclic voltammetry of complex 1 (1 mM) in 0.1 M *n*-$Bu_4NPF_6$/MeCN with and without $CH_3COOH$ (0–12 mM) at a scan rate of 0.1 V $s^{-1}$

acid (Fig. 4). The dramatic increment of the current intensity (reduction potential at −1.875 V for complex **1** or at −2.355 V for complex **2**) with increasing concentration of acid is indicative of a catalytic proton reduction process [31–33]. Because protonation at the Fe–Fe center or at the peripheral N atom of the diiron dithiolate core can positively shift the reduction potential by about 1 or 0.4 V, respectively [34], the less negative reduction potential (at −1.875 or −2.355 V in the presence of $CF_3COOH$ or $CH_3COOH$) may not result from protonation of the Fe–Fe center. This means that the bridging or terminal hydride intermediate in the presence of $CF_3COOH$ or $CH_3COOH$ cannot be produced [35]. At the present stage, the exact catalytic mechanism in the presence of $CF_3COOH$ (moderate acid, $pK_a = 12.7$ in $CH_3CN$) or $CH_3COOH$ (weak acid, $pK_a = 22.3$ in $CH_3CN$) [36, 37] cannot be inferred with confidence. Complex **2** displays two irreversible reduction processes at −2.154 and −2.551 V, an irreversible oxidation process at +0.342 V, respectively (Fig. 5).

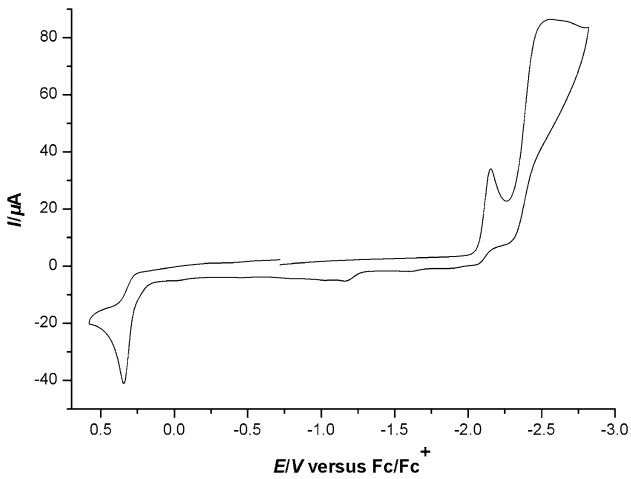


**Fig. 5** Cyclic voltammetry of complex **2** (1 mM) in 0.1 M *n*-$Bu_4NPF_6$/MeCN at a scan rate of 0.1 V $s^{-1}$

## Conclusions

Substitution of two carbonyls of the all-carbonyl diiron propanedithiolate complex $[\mu\text{-}(SCH_2)_2CHC_6H_5]Fe_2(CO)_6$ with bidentate phosphine ligands, namely *cis*-dppv and $(Ph_2P)_2$N-Pr-*n*, yielded an asymmetrically substituted complex **1** and a symmetrically substituted complex **2** under different reaction conditions. In the solid state, the two phosphine atoms of *cis*-dppv chelate one of the two iron atoms of complex **1** with a basal–apical coordination geometry, whereas the two phosphine atoms of $(Ph_2P)_2$N-Pr-*n* coordinate the two iron atoms of complex **2** in a bridging basal–basal manner. Moderate acid (trifluoroacetic acid) or weak acid (acetic acid) positively shifted the reduction potential of complex **1** by ca. 0.2 V. Complex **1** can catalyze reduction of protons to dihydrogen under electrochemical conditions.

## Supporting data

CCDC 974591 (complex **1**) and 974593 (complex **2**) contain the supplementary crystallographic data for this paper. These data can be obtained free of charge from The Cambridge Crystallographic Data Centre via www.ccdc.cam.ac.uk/data_request/cif.

**Acknowledgments** This work is financially supported by the Chinese National Natural Science Foundation (No. 21072046) and the Chinese National Training Programs of Innovation and Entrepreneurship for Undergraduates (No. 201210467022).

## References

1. Albracht SP (1994) J Biochim Biophys Acta Bioenerg 1188:167
2. Graf EG, Thauer RK (1981) FEBS Lett 136:165
3. Cammack R, Patil D, Aguirre R, Hatchikian EC (1982) FEBS Lett 142:289
4. Peters JW, Lanzilotta WN, Lemon BJ (1998) Science 282:1853
5. Nicolet Y, Piras C, Legrand P, Hatchikian EC, Fontecilla-Camps JC (1999) Structure 7:13
6. Nicolet Y, De Lacey AL, Vernède X, Fernandez VM, Hatchikian EC, Fontecilla-Camps JC (2001) J Am Chem Soc 123:1596
7. Pierik AJ, Hulstein M, Hagen WR, Albracht SPJ (1998) Eur J Biochem 258:572
8. De Lacey AL, Stadler C, Cavazza C, Hatchikian EC, Fernandez VM (2000) J Am Chem Soc 122:11232
9. Chen Z, Lemon BJ, Huang S, Swartz DJ, Peters JW, Bagley KA (2002) Biochemistry 41:2036
10. Wang N, Wang M, Wang Y, Zheng DH, Han HX, Ahlquist MSG, Sun LC (2013) J Am Chem Soc 135:13688
11. Manor BC, Rauchfuss TB (2013) J Am Chem Soc 135:11895
12. Felton GAN, Vannucci AK, Chen JZ, Lockett LT, Okumura N, Petro BJ, Zakai UI, Evans DH, Glass RS, Lichtenberger DL (2007) J Am Chem Soc 129:12521
13. Borg SJ, Behrsing T, Best SP, Razavet M, Liu XM, Pickett CJ (2004) J Am Chem Soc 126:16988
14. Mejia-Rodriguez R, Chong D, Reibenspies JH, Soriaga MP, Darensbourg MY (2004) J Am Chem Soc 126:12004
15. Wang WG, Nilges MJ, Rauchfuss TB, Stein M (2013) J Am Chem Soc 135:3633
16. Liu XF, Xiao XW, Shen LJ (2011) Transit Met Chem 36:465
17. Darensbourg MY, Lyon EJ, Smee JJ (2000) Coord Chem Rev 206–207:533
18. Evans DJ, Pickett CJ (2003) Chem Soc Rev 32:268
19. Fontecilla-Camps JC, Volbeda A, Cavazza C, Nicolet Y (2007) Chem Rev 107:4273
20. Gloaguen F, Rauchfuss TB (2009) Chem Soc Rev 38:100
21. Tye JW, Darensbourg MY, Hall MB (2006) Inorg Chem 45:1552
22. Li CG, Zhu Y, Jiao XX, Fu XQ (2014) Polyhedron 67:416
23. Ewart G, Lane AP, McKechnie J, Payne DS (1964) J Chem Soc 1543
24. Dolomanov OV, Bourhis LJ, Gildea RJ, Howard JAK, Puschmann H (2009) J Appl Cryst 42:339
25. Sheldrick GM (2008) Acta Cryst A64:112
26. Collman JP, Hegedus LS (1980) Principles and applications of organotransition metal chemistry. University Science Books, Mill Valley, pp 81–89
27. Crabtree RH (2005) The organometallic chemistry of the transition metals, 4th edn. Wiley, New York
28. Yam VWW, Fung WKM, Wong MT (1997) Organometallics 16:1772
29. Justice AK, Zampella G, Gioia LD, Rauchfuss TB, van der Vlugt JI, Wilson SR (2007) Inorg Chem 46:1655
30. Adam FI, Hogarth G, Richards I (2007) J Organomet Chem 692:3957
31. Chong D, Georgakaki IP, Mejia-Rodriguez R, Sanabria-Chinchilla J, Soriaga MP, Darensbourg MY (2003) Dalton Trans 4158
32. Borg SJ, Behrsing T, Best SP, Razavet M, Liu X, Pickett CJ (2004) J Am Chem Soc 126:16988
33. Gloaguen F, Lawrence JD, Rauchfuss TB (2001) J Am Chem Soc 123:9476
34. Felton GAN, Mebi CA, Petro BJ, Vannucci AK, Evans DH, Glass RS, Lichtenberger DL (2009) J Organomet Chem 694:2681
35. Ezzaher S, Capon JF, Gloaguen F, Pétillon FY, Schollhammer P, Talarmin J (2007) Inorg Chem 46:3426
36. Felton GAN, Glass RS, Lichtenberger DL, Evans DH (2006) Inorg Chem 45:9181
37. Wang M, Chen L, Sun LC (2012) Energy Environ Sci 5:6763